Journal of Energy Storage xxx (2016) xxx–xxx

Contents lists available at ScienceDirect

Journal of Energy Storage

journal homepage: www.elsevier.com/locate/est

Gas-to-gas heat exchanger design for high performance thermal energy storage

B. Cárdenas*, S.D. Garvey, B. Kantharaj, M.C. Simpson

Department of Mechanical, Materials and Manufacturing Engineering, University of Nottingham, United Kingdom

ARTICLE INFO

Article history:
Received 5 October 2016
Received in revised form 25 January 2017
Accepted 1 March 2017
Available online xxx

Keywords:
Air to air heat exchanger
High exergy efficiency
Non-constant cross sectional area
Additive manufacturing
Cost optimization

ABSTRACT

The mathematical modelling and optimization of a gas-to-gas heat exchanger with a non-constant cross sectional area is presented. The design of the cross sectional area of the heat exchanger analyzed is based on an hexagonal mesh, which would be highly impractical to fabricate in a conventional way but could be built relatively easily through modern manufacturing techniques. The geometric configuration proposed allows attaining a high exergy efficiency and a significant cost reduction, measured in terms of volume per unit of exergy transfer. The relationship that exists between the overall exergy efficiency of the heat exchanger and its cost is thoroughly explained throughout the study.

The results obtained from the modelling demonstrate the premise that it is possible to realize designs for heat exchangers that are highly exergy-efficient and very cheap, owing to the small volume of material required, if the constrains imposed by the limitations of traditional manufacturing methods are set aside. Furthermore, the study reveals a very important fact: the volume of material in a heat exchanger increases in quadratic proportion to its characteristic dimension, which implies that scaling up the geometry has a strong impact on its cost-effectiveness.

© 2017 Elsevier Ltd. All rights reserved.

1. Introduction

Heat exchangers (HX) are extensively used in diverse industrial processes nowadays. Several different types of heat exchangers have been developed for different applications; being the shell-and-tube and plate-fin the most commonly utilized configurations [1].

The design of a HX involves a number of highly interdependent geometric and operating variables that often exhibit trade-offs [2] however, through a careful selection of parameters cost-effective designs with a high efficiency can be realized. This is of great importance for the industry and in particular, for the development and widespread deployment of utility-scale energy storage technologies, such as compressed air energy storage (CAES) systems.

A vast amount of research has been dedicated in past years to develop design strategies for achieving substantial reductions in the cost of a HX. The use of evolutionary algorithms and other population-based optimization methods for minimizing the total cost of HXs has been studied by many researchers. Following a literature review can be found, in which examples of the work aimed at optimizing the design of HXs in terms of maximizing performance and/or minimizing cost carried out by different authors are discussed.

Sanaye and Hajabdollahi carried out by means of a genetic algorithm the optimization in terms of cost and effectiveness of a shell-and-tube HX [3] and a plate-fin HX [4] presenting in both studies a set of multiple optimum solutions (Pareto front) for the objective functions. In a different study, Hajabdollahi et al. [5] used a genetic algorithm to optimize a compact plate-fin HX in terms of effectiveness and pressure drops. The authors observed that any geometric change that reduces pressure drops in the optimum situation has a negative impact in the effectiveness of the HX and vice versa, therefore a set of Pareto optimal solutions was presented. Similarly, Najafi et al. [6] carried out the optimization of a HX of the same type, albeit focusing on different objective functions. The researchers provide a number of Pareto optimal solutions, which exhibit the trade-off that exists between the maximum total rate of heat transfer and the minimum total cost of the component.

Patel and Rao used a particle swarm optimization (PSO) algorithm to minimize the total annual cost of a shell-and-tube [7] and a plate-fin HX [8]. Several different case studies are presented through which the effectiveness and accuracy of the

* Corresponding author.
E-mail address: Bruno.Cardenas@nottingham.ac.uk (B. Cárdenas).

http://dx.doi.org/10.1016/j.est.2017.03.004
2352-152X/© 2017 Elsevier Ltd. All rights reserved.

Please cite this article in press as: B. Cárdenas, et al., Gas-to-gas heat exchanger design for high performance thermal energy storage, J. Energy Storage (2017), http://dx.doi.org/10.1016/j.est.2017.03.004

Nomenclature

Acronyms

HP	high pressure
HX	heat exchanger
LP	low pressure

Symbology

A	cross sectional area (m^2)
A_s	heat transfer area (m^2)
$\overline{B}$	mean exergy transfer (W/m)
$\dot{B}_{HP}$	exergy of the heat at the HP side (W/m)
$\dot{B}_{LP}$	exergy of the heat at the LP side (W/m)
$\dot{B}_{LOSS}$	total exergy losses (W/m)
$\dot{B}_{LQ}$	exergy loss due to heat transfer (W/m)
$\dot{B}_{\Delta P}$	exergy loss due to pressure drop (W/m)
$\dot{B}_{\Delta HP}$	exergy loss due to pressure drop in the HP side (W/m)
$\dot{B}_{\Delta LP}$	exergy loss due to pressure drop in the LP side (W/m)
C_P	specific heat capacity (J/kg K)
ΔP	pressure drop per unit length (Pa/m)
ΔP_{HP}	pressure drop in the HP side (Pa/m)
ΔP_{LP}	pressure drop in the LP side (Pa/m)
ΔT	temperature delta from T_{avg} (K)
D	distance between centres of HP pipes (m)
ε	roughness height (m)
$\varepsilon/\emptyset$	relative pipe roughness
f_D	Darcy–Weisbach friction factor
h	convection coefficient (W/m^2 K)
k_{air}	thermal conductivity of air (W/m K)
k_{wall}	thermal conductivity of wall (W/m k)
λ	fraction of HP pipe perimeter covered by flanges
L	height of the flange (m)
μ	dynamic viscosity of air (Pa s)
$\dot{m}_{HP}$	mass flow rate per HP pipe (kg/s)
$\dot{m}_{LP}$	mass flow rate per LP pipe (kg/s)
n	number of rings of HP pipes
Nu	Nusselt number
$\emptyset$	pipe diameter (m)
ψ	fraction of the pipe being analyzed
p	perimeter of flow area of pipe (m)
P	pressure (Pa)
P_{HP}	pressure of the HP side (Pa)
P_{LP}	pressure of the LP side (Pa)
Pr	Prandtl number
$\dot{Q}$	heat transfer rate per unit length (W/m)
ρ	density of air (kg/m^3)
r_{HP}	radius of the HP pipe (m)
Re	Reynolds number
S	allowable stress of pipe material (Pa)
t_{HP}	thickness of HP pipes (m)
t_{LP}	thickness of the flange at the base (m)
t_{mf}	thickness of the flange at midpoint (m)
T_{amb}	ambient temperature (K)
T_{avg}	average temperature of HX section (K)
T_{HP}	temperature of the HP stream (K)
T_i	temperature of inner wall of HP pipe (K)
T_{LP}	temperature of the LP stream (K)
T_{mf}	temperature of the flange at middle (m)
T_O	temperature of outer wall of HP pipe (K)
$T(x)$	temperature at a point x in flange (K)
∇T	temperature gradient of HX segment (K/m)
U	mean flow velocity of air (m/s)
$V/\overline{B}$	volume of material per unit exergy transfer (m^3/kW)
W	exergy efficiency
X	ratio of proportional pressure drops
Y	ratio of temperature differences
Z	fraction of total exergy losses caused by pressure drops

algorithm is demonstrated. The results show an improvement with respect to the results obtained by previous researchers via more standard genetic algorithms. Furthermore, Sadeghzadeh et al. [9] presented a comparison between the PSO and a genetic algorithm for the optimization of a shell-and-tube HX in terms of cost, expressed as a function of surface area and power consumption. The PSO method produced superior results for the problem, which supports the conclusions from Patel and Rao [7,8].

Some authors have explored the use of variants of the PSO method. Mariani et al. [10] optimized the design of a shell-and-tube HX through a quantum PSO algorithm. The researchers reported that considerable reductions in capital investment (~20%) and annual pumping cost (~72%) were achieved. Turgut [11], on the other hand, investigated the use of a hybrid-chaotic PSO algorithm for the multi-objective optimization of a plate-fin HX in terms of heat transfer area, total pressure drops and total cost. The author observed that the PSO algorithm produced more accurate results than many other optimization algorithms discussed in the literature.

Besides the techniques aforementioned, several other evolutionary and population based optimization algorithms have been used by many researchers for optimizing the design of HXs from different perspectives such as the imperialist-competitive, cuckoo-search, biogeography-based optimization, teaching-learning and firefly algorithms, among others.

Hadidi et al. [12] optimized the design of a shell-and-tube HX by means of an imperialist-competitive algorithm. The authors achieved reductions in capital cost of up to 6.1% with respect to selected reference cases. Yousefi et al. [13] used an improved harmony-search algorithm to optimize the design of a plate-fin HX with aims at minimizing heat transfer area and pressure drops. The results obtained indicate that the approach studied can produce more accurate solutions than genetic and PSO algorithms.

Wang and Li [14] carried out a multi-objective optimization (maximizing efficiency and minimizing cost) of a plate-fin HX via a cuckoo-search algorithm (CSA). The authors reported satisfactory results and concluded that the CSA method is capable of generating more accurate solutions than single-objective approaches while requiring less iterations. Likewise, Asadi et al. [15] used a CSA for the minimization of the cost of a shell-and-tube HX. The authors achieved reductions in cost of 9.4% and 13.1% with respect to results produced by genetic and PSO algorithms, respectively.

Hadidi and Nazari [2] carried out a cost optimization of a HX through a biogeography-based optimization (BBO) algorithm with which reductions in capital investment and operating costs in comparison to literature reference cases of up to 14% and 96%, respectively, were achieved. Patel and Savsani [16] and Rao and Patel [17] carried out, by means of a modified version of the teaching-learning algorithm, a multi-objective optimization focused on effectiveness and total cost of a shell-and-tube and a plate-fin HX, respectively. The authors reported that better Pareto optimal solutions were attained than those found by generic algorithms for an analogous problem.

More recently, Mohanty [18] published the results of the cost optimization of a shell-and-tube HX carried out via a firefly algorithm. The study shows that the total surface area and total cost can be reduced by 27% and 29%, respectively, with respect to the reference designs. Furthermore, the study presents a comparison of the firefly algorithm against some of the aforementioned

Please cite this article in press as: B. Cárdenas, et al., Gas-to-gas heat exchanger design for high performance thermal energy storage, J. Energy Storage (2017), http://dx.doi.org/10.1016/j.est.2017.03.004

optimization techniques such as GA, PSO, CSA and BBO, which suggests that the firefly algorithm is the most effective method for the cost-optimization of the design of a HX.

It is clear that a substantial amount of research has been carried out with the end goal of reducing the total cost of HXs; numerous researchers have studied several different optimization algorithms through the use of which very good results can be achieved. All the optimization techniques abovementioned can achieve considerable reductions in cost despite the fact that their outputs are restricted by a pre-conceived design; however, better results could be achieved by the optimization process if the starting point (design) was better.

The heat exchangers that are currently used by the industry were designed decades ago under the limitations of the fabrication methods of those times. Nevertheless, there is a much wider range of manufacturing techniques available nowadays, such as additive manufacturing, that are capable of producing much more complex designs, through which higher efficiencies and/or lower costs can be achieved. Hence, research efforts should be focused on developing innovative designs of HXs, not based on existing ones, that exploit the capabilities of modern manufacturing.

Accordingly, this work propounds and investigates the use of an intricate geometry, which would be highly unpractical to fabricate by traditional methods, for a gas to gas heat exchanger with aims at obtaining designs that simultaneously maximize the exergy efficiency and minimize the cost. The main difference between the present study and the investigations discussed before is that rather than simply trying to tune geometric and/or operational parameters of an existing design of HX to achieve a reduction in the cost of the equipment, a rather radial design is proposed as the starting point. It is important to highlight that this work focuses particularly on understanding the trade-off that exists between the overall exergy efficiency of the HX and its cost.

2. Geometric design of the gas-to-gas HX

Generally, HXs have a constant cross-sectional area throughout their whole length; however, it would be much better to have a HX with graded properties. The approach followed in the present work for finding the optimum geometry, in terms of maximum efficiency and minimum cost, is to design a HX with a non-constant cross-sectional area between the hot and cold ends. For this purpose, the length of the HX is divided into n different segments (or slices) and each segment is designed specifically for the temperature range at which it will operate.

The body of the heat exchanger can be regarded as series of segments whose dimensions adjust with length. Each segment has a constant cross-section throughout its length (which should be relatively small) however, geometric parameters change from one segment to the next. Therefore, the properties of the HX as a whole are modified in discrete steps rather than varying continuously with length; although, there is no reason why the latter could not be the case.

The cross-sectional area of each of the segments is based on an hexagonal mesh (honeycomb pattern). This geometry was chosen because it has multiple axes of symmetry, which allows analysing a small section of it assuming that a similar behaviour can be observed elsewhere.

The low pressure (LP) and high pressure (HP) pipes are distributed so that each HP pipe is surrounded by six LP pipes whereas each LP pipe is surrounded by three HP pipes, as shown by Fig. 1. The cross-sectional area of the segment of HX starts as a fully hexagonal mesh. The regions corresponding to the HP pipes are transformed into circles, because a cylinder is the best geometric shape for a pipe that will handle pressurized fluids, the outer wall of these pipes is also rounded (although it could remain straight) to make an efficient use of material.

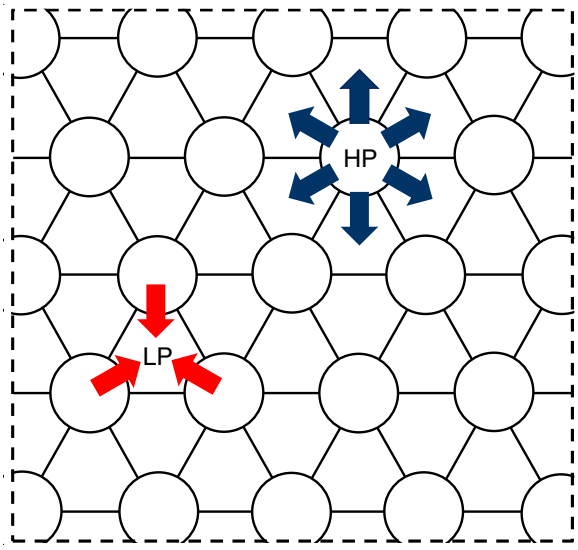

The arrows in Fig. 1 show the heat flows assumed for the modelling. Each HP pipe delivers heat to the six adjacent LP pipes whereas each LP pipe receives heat from the three HP pipes around it. It is assumed that no interaction occurs between contiguous LP pipes. An advantageous property of the geometry upon which the cross-sectional design is based is that it grows in concentric rings, as shown by Fig. 2. This characteristic allows adding rings of HP pipes at the perimeter of the cross section to increase the capacity of the HX without modifying its behaviour. The number of HP and LP pipes in the arrangement, according to the number of rings (n), is given by Equations (1) and (2), respectively.

$$HP = 1 + \sum_{i=1}^{n} 6i \tag{1}$$

$$LP = \sum_{i=1}^{n} 12i - 6 \tag{2}$$

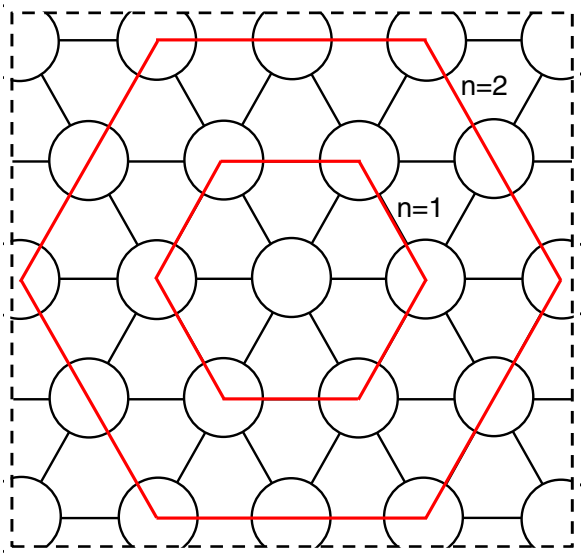

Fig. 2. Growth of the cross-section of the HX in concentric rings.

Please cite this article in press as: B. Cárdenas, et al., Gas-to-gas heat exchanger design for high performance thermal energy storage, J. Energy Storage (2017), http://dx.doi.org/10.1016/j.est.2017.03.004

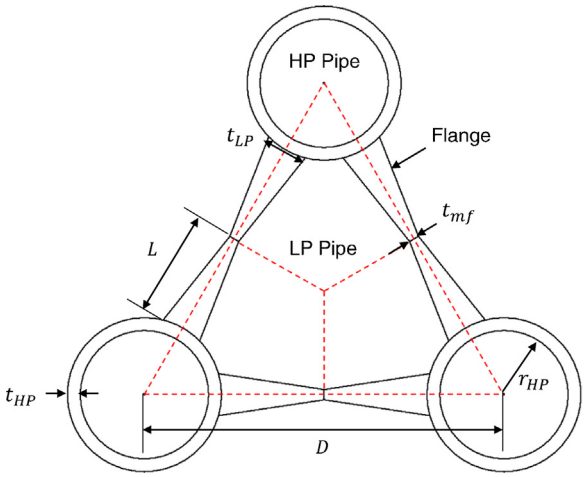

Fig. 3. Section consisting of 3 HP pipes and the LP comprised between them.

A section of the geometry consisting of three HP pipes and the LP pipe comprised between them is shown in Fig. 3. As it can be seen, the walls of the LP pipe are made by trapezoidal elements, which will be referred to as "flanges" henceforth. It is assumed that the LP stream of the gas to gas HX will be at ambient (or marginally higher) pressure; therefore, the flanges do not have a thickness requirement to withstand pressure. The thinnest possible wall is desirable from a material utilization standpoint; however, the flanges need to be thick enough to hold the structure together and to transport heat from the wall of the HP pipe to the LP stream. Stated differently, their sizing is conduction driven rather being dictated by pressure.

There are five geometric parameters that define the geometry, as can be seen in Fig. 3: The distance between centres of HP pipes (D), the radius (r_{HP}) and thickness (t_{HP}) of the HP pipes, the thickness of the flange at the base (t_{LP}) and the thickness of the flange at middle height (t_{mf}). For simplicity, the thickness of the flange at middle height is somewhat arbitrarily defined to be a fifth of the thickness at the base.

3. Mathematical modelling of an HX segment

The objective is, as aforementioned, to find an optimum design in terms of cost per unit of exergy transfer for the cross-sectional area of a specific segment of a HX for the temperature range at which it will operate. One of the main cost driving factors in an additive manufacturing process is the cost of the material utilized; hence achieving reductions in the effective volume of the design is a good approach towards minimizing the total cost of the equipment. The mathematical model and algorithm developed are focused on the design and optimization of only 1 segment of the HX. The optimization of the whole body of a HX can be done by applying the same algorithm to each one of the n segments in the structure and optimizing them for their corresponding operating temperature.

An exhaustive search based on testing every possible combination of variables to find the optimum design is unquestionably not a good approach because a great deal of all possible combinations of variables will fail to meet the required performance or may be physically unrealizable, in addition of being computationally expensive. Therefore, an organized approach to explore the multidimensional space containing the solution is required.

Although seemingly counterintuitive, four additional variables, named W, X, Y and Z are introduced. These variables help to constrain the multidimensional space by relating two or more operational parameters of the HX segment between them. The new variables are defined in the following way:

- W is the desired exergy efficiency of the HX segment. In this study efficiencies in the range of 97–99% are evaluated. This parameter defines indirectly the average temperatures of the HP and LP streams, as it will be explained further on.
- X, given by Eq. (3), is the ratio of proportional pressure drops (ΔP) between the two air streams.
- Y, given by Eq. (4), describes the temperature drop along the flanges of the structure.
- Z, given by Eq. (5), is the ratio of the exergy losses due to pressure drops with respect to the total exergy losses.

$$X = \left(\frac{\Delta P_{HP}}{P_{HP}}\right) / \left(\frac{\Delta P_{LP}}{P_{LP}}\right) \tag{3}$$

$$Y = \frac{T_{mf} - T_{Lp}}{T_o - T_{LP}} \tag{4}$$

$$Z = \frac{B_{\Delta HP} + B_{\Delta LP}}{B_{LOSS}} \tag{5}$$

The four previously described factors are called "slow moving variables" because their value changes little in comparison with the rest of the (fast moving) variables in the space such as D, r_{HP}, t_{LP} and $\dot{m}$; thus it is possible to define their value arbitrarily and still approximate a good solution. The values of the slow moving variables can be subsequently fine-tuned to achieve a further reduction in the volume of material required per unit of exergy transfer.

A challenge encountered within the present study is that all the variables are highly interdependent between them; whereby the implementation of an iterative process to search for the solution is necessary. The algorithm developed for this purpose consists of three iterative loops, one that determines the radius and wall thickness of the HP pipes so that the proportional pressure drops satisfy Eq. (3), a second one that determines the thickness of the flanges based on Eq. (4) and a third outer one that encompasses the previous two and adjusts the mass flow rates so that Eq. (5) is met. The process followed by the algorithm is graphically explained in Fig. 4.

The distance between centres of HP pipes (D) is the fast moving variable that is used as the characteristic dimension. Different designs are obtained for a number of different values of D and compared between them to find the best performing configuration. An initial set of parameters has to be provided to the algorithm before any calculations are performed. This set comprises:

- The average temperature at which the HX segment will be operating (T_{avg})
- The pressures of the HP and LP streams (P_{HP} and P_{LP}, respectively)
- Thermal conductivity (k_{wall}) and allowable stress (S) of the material of the construction

After the initial parameters, the values of the slow moving variables W, X, Y and Z are defined, as well as the D for which a design will be obtained. The temperatures of the HP and LP fluids are given by W, Z and T_{avg} through the following set of equations:

$$\dot{B}_{LP} = \dot{Q} \cdot \left(1 - \frac{T_{amb}}{T_{avg} - \Delta T}\right) \tag{6}$$

Please cite this article in press as: B. Cárdenas, et al., Gas-to-gas heat exchanger design for high performance thermal energy storage, J. Energy Storage (2017), http://dx.doi.org/10.1016/j.est.2017.03.004

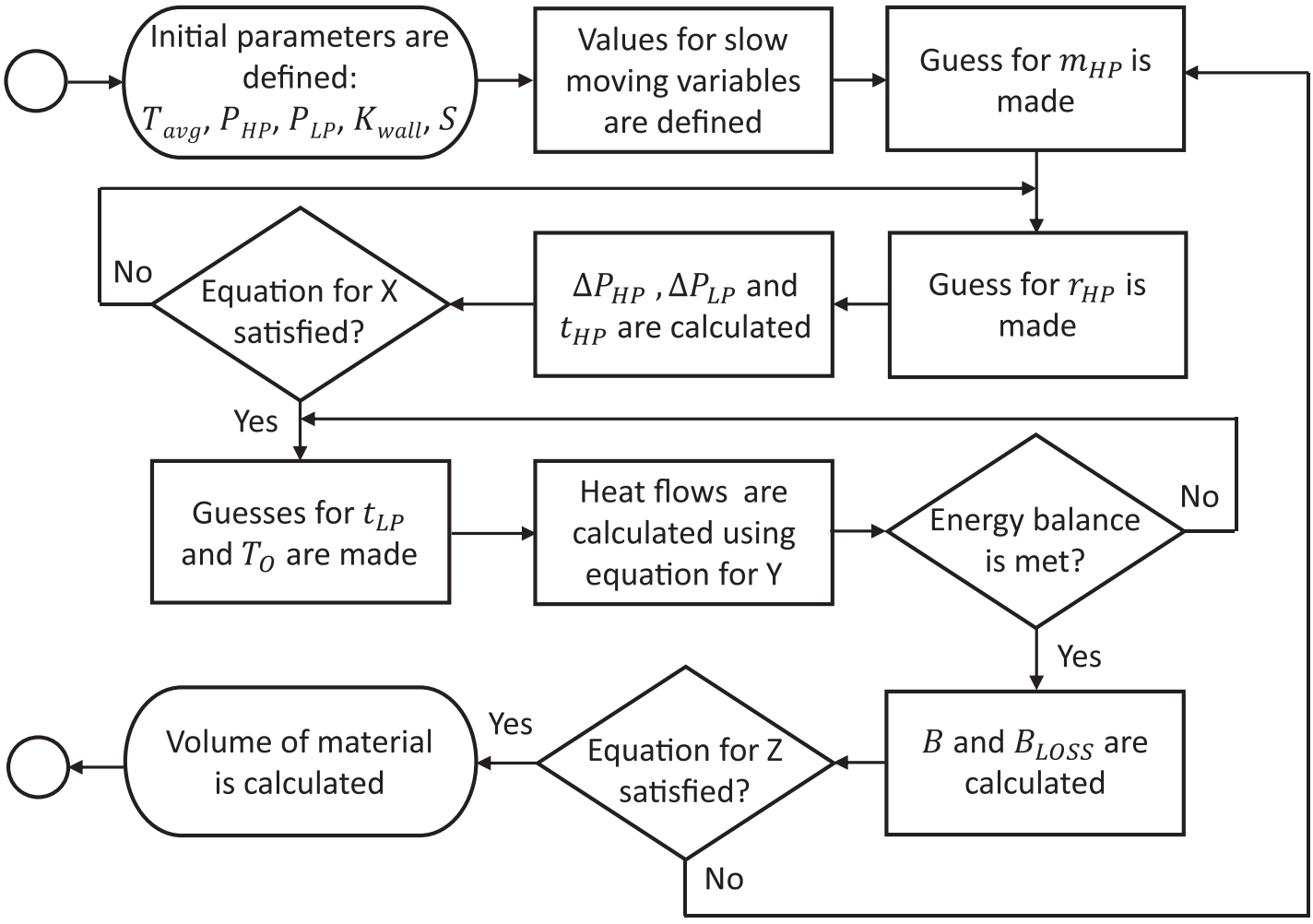

Fig. 4. Algorithm used for the calculations.

$$\dot{B}_{Hp} = \dot{Q} \cdot \left(1 - \frac{T_{amb}}{T_{avg} + \Delta T}\right) \tag{7}$$

$$\overline{B} = \frac{\dot{B}_{LP} + \dot{B}_{Hp}}{2} \tag{8}$$

$$(1 - W) \cdot (1 - Z) = \dot{B}_{HP} - \dot{B}_{LP}\overline{B} \tag{9}$$

$$T_{HP} = T_{avg} + \Delta T \tag{10}$$

$$T_{LP} = T_{avg} - \Delta T \tag{11}$$

The first step of the calculation process is to take a guess for the mass flow rates. The HX has equal mass flow rates in both directions, which is very convenient from an engineering point of view. Therefore, the mass flow rate in a HP pipe ($\dot{m}_{HP}$) is double than the mass flow rate in a LP pipe ($\dot{m}_{LP}$) because there are twice as many LP pipes than HP pipes. It is also important to highlight that performance parameters in the calculations are expressed per unit length, as the length of the segment of HX is left undefined.

The radius of the HP pipe (r_{HP}) is determined by the first iterative loop of the algorithm so that the proportional pressure drops of both streams satisfy Eq. (3) for the X defined. For clarity, a value of 1 for X means that the proportional pressure drops of both streams are equivalent while if X >1 the proportional pressure losses in the HP stream are greater than in the LP stream. First, a guess for r_{HP} is made; then the pressure drops (ΔP) per unit length inside the pipes are calculated based on this value by means of Equation (12) [19]. The friction factor (f_D) is calculated through Eq. (13), which is an approximation to the iterative Colebrook equation [20]. The accuracy of the friction factor obtained from this equation has an error margin of ±2% for Reynolds numbers greater than 3000 [21].

$$\Delta P = f_D \cdot \rho \cdot U^2 \cdot (2\phi)^{-1} \tag{12}$$

$$f_D = \left(-1.8 \cdot \log_{10} \cdot \left[(\varepsilon/3.7\emptyset)^{1.1} + 6.9 \cdot Re^{-1}\right]\right)^{-2} \tag{13}$$

The case of the HP stream is calculated first. At this point t_{HP} is also determined, by means of Eq. (14). The thickness of the pipe depends on the pressure of the fluid and on the allowable stress (S) of the material [22]. It should be mentioned that the allowable stress is a fixed value defined at the beginning of the calculations, therefore the optimization algorithm cannot generate designs that do not have a wall thick enough to hold the pressure of the HP stream. Next, the pressure drop on the LP side is calculated. Given

Please cite this article in press as: B. Cárdenas, et al., Gas-to-gas heat exchanger design for high performance thermal energy storage, J. Energy Storage (2017), http://dx.doi.org/10.1016/j.est.2017.03.004

that the cross sectional area of the LP pipe is not circular, an equivalent hydraulic diameter has to be calculated through Eq. (15).

$$t_{HP} = \frac{r_{HP} \cdot P_{HP}}{S - P_{HP}} \tag{14}$$

$$\phi_h = 4A/p \tag{15}$$

The value of r_{HP} is updated and the calculations are repeated until the values obtained for the proportional pressure drops on both sides satisfy Eq. (3) for the value of X defined. Subsequently, the second iterative loop of the algorithm calculates the required thickness for the flanges. This is done through a double iteration with T_O, which is the temperature of the outer wall of the HP pipe, and t_{LP}, which is the thickness of the base of the flange. Guesses are made for both variables and a T_{mf} is found such that Eq. (4) is satisfied for the value of Y defined. The flange is assumed to have an internal temperature gradient described by Eq. (16) [23].

$$T(x) = Y \cdot (T_O - T_{LP}) \cdot \cosh\left(\cosh^{-1}\left(\frac{1}{Y}\right) \cdot \frac{L - x}{L}\right) + T_{LP} \tag{16}$$

As aforementioned, the air in each LP pipe is heated by the air flowing through three different HP pipes. Due to the symmetry of the hexagonal mesh it is possible to assume that 1/6 of the air in a HP pipe interacts with 1/3 of the air in a LP pipe and that the mass of LP air contained in that 1/3 of pipe does not interact with remaining 2/3 of LP air. With basis on this assumption, it is possible to divide the geometry even further, as shown in Fig. 5, so that only a 1/12 of a HP pipe and a 1/6 of a LP pipe are analyzed.

It is important to keep in mind that the behaviour of the HP pipes of the outer ring of the cross-section of the HX is slightly different from what is observed in the rest of the pipes of the HX. This is due to the fact that in the case of the HP pipes of the outer ring only 2/6 of their surface is surrounded by LP pipes (the remaining 4/6 would be probably insulated in a practical application) whereas the rest of the HP pipes of the HX are completely surrounded by LP pipes. Consequently, the approach of only focusing on a very small section of the cross-sectional area of the HX for the calculations (as shown in Fig. 5) is only valid if the HX is made up by a large number of rings ($n > 12$) so that the difference in conditions at the outer ring does not have a significant effect on the results obtained.

The heat flows (per unit length of HX) inside this fraction of the geometry are calculated by means of the one dimensional conduction equation (Eq. (17)) and the convection equation (Eq. (18)) as appropriate.

$$\dot{Q} = \frac{k \cdot A \cdot \delta T}{\delta x} \tag{17}$$

$$\dot{Q} = h \cdot A_s \cdot \delta T \tag{18}$$

For example, $\dot{Q}_3$ is a heat flow by conduction from the wall of the HP pipe to the flange, which is determined by the thermal conductivity of the material of the construction, the height of flange up to its middle point (L), the cross-sectional area of the flange (important to note that due to the shape, this area is not constant along the height of the flange), the temperature difference between the outer surface of the HP pipe (T_o) and the temperature of the flange at middle height (T_{mf}). On the other hand, $\dot{Q}_2$ is a heat flow by convection from the wall of the HP pipe to the LP fluid, which is determined by the temperature difference between the outer surface of the HP pipe and the mean temperature of the LP fluid, the contact area between the HP pipe wall and the LP fluid and a heat transfer coefficient (h).

The heat transfer coefficients are calculated through Eq. (19). It is worth mentioning again that for the case of the LP stream an equivalent hydraulic diameter should be used as the pipe is not cylindrical.

$$h = \frac{Nu \cdot k_{air}}{\phi} \tag{19}$$

where

$$Nu = 0.023 \cdot Re^{0.8} \cdot pr^{0.33} \tag{20}$$

$$\mathrm{Re} = \frac{m \cdot \phi}{\mu \cdot A} \tag{21}$$

$$\mathrm{Pr} = \frac{\mu \cdot C_p}{k_{air}} \tag{22}$$

The specific heat capacity of the air (C_P) is calculated through the equation proposed by Lemmon et al. [24] while the dynamic viscosity (μ) and thermal conductivity (k_{air}) are calculated through the Lemmon and Jacobsen equations [25].

If an energy balance in this section is not met, the values for t_{LP} and T_O are revised and calculations are repeated. At this point, the geometry has been completely characterized and the heat flows are known, thus it is possible to calculate the temperature gradient of the HX segment through Eq. (23), where ψ is the fraction of the pipe being analyzed (1/12 for the case of HP pipes and 1/6 for the case of LP pipes). The exergy losses due to pressure drops can be calculated through Eq. (24), the exergy losses due to heat transfer by means of Eq. (25), the total exergy losses (26) while the mean exergy transfer is given by Eq. (8).

$$\nabla T = \frac{\dot{Q}}{\dot{m} \cdot (\psi) \cdot C_p} \tag{23}$$

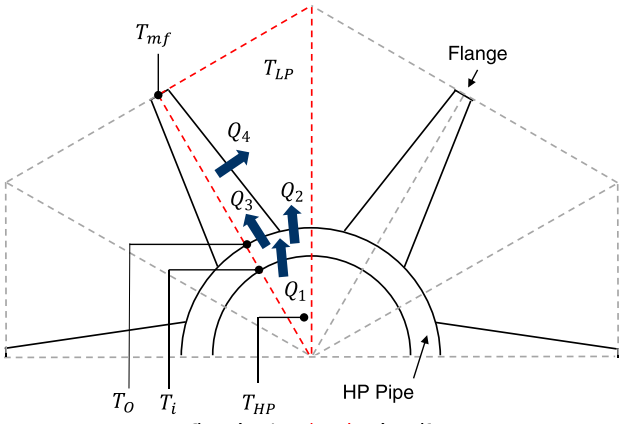

Fig. 5. Section of the geometry used for analysis comprised by 1/12 of the HP pipe and 1/6 of the LP pipe.

Table 1
Set of initial parameters for the case study.

Slow moving variables		Properties of air		Properties of steel	
W	0.97, 0.98 & 0.99	T_{avg}	745 K & 400 K	K_{wall}	See Eq. (27) (W/mK)
X	1.0	T_{amb}	290 K	S	110.6 MPa
Y	0.5	P_{HP}	5 MPa	$\varepsilon/\emptyset$	0.005
Z	0.5	P_{LP}	101.325 kPa		

$$\dot{B}_{\Delta P} = (\psi) \cdot \dot{m} \cdot R \cdot T_{amb} \cdot (\Delta P/P) \tag{24}$$

$$\dot{B}_{LQ} = \dot{B}_{HP} - \dot{B}_{LP} \tag{25}$$

$$\dot{B}_{LOSS} = \dot{B}_{LQ} + \dot{B}_{\Delta HP} + \dot{B}_{\Delta LP} \tag{26}$$

If Eq. (5), which dictates the relationship between exergy loses due to pressure drops in both streams with respect to total exergy losses is not satisfied, the values for $\dot{m}_{HP}$ and $\dot{m}_{LP}$ are revised and the whole process is carried out again. After knowing the value of $\overline{B}$ it is possible to calculate the volume of material required per unit of exergy transfer, which is the objective function of the optimization.

4. Analysis of results obtained and discussion

A case study carried out through the algorithm previously described is presented and thoroughly analyzed in the current section. The material selected for the structure of the HX is a typical stainless steel, whose thermal conductivity is given by Eq. (27). Materials with a higher thermal conductivity or lower cost could be used.

$$K_{wall} = 25.5 + \frac{T_{avg}}{80} - \frac{T_{avg}^2}{120 \times 10^3} \tag{27}$$

20 different designs corresponding to 20 different values of D, going from 0.01 m to 0.25 m, were generated. This allows understanding the behaviour of different performance metrics of the HX as it is scaled up and choosing the configuration that attains the highest exergy transfer per unit volume. Two different average temperatures are analyzed: 745 K and 400 K. One of the envisaged applications for a HX of this kind are compressed air energy storage systems in which a high exergy efficiency of the components is of paramount importance. Typically these systems produce streams of compressed air at pressures in the range of 5–7 MPa and temperature in the range of 770–800 K. A segment of HX operating at an average temperature of 745 K would be near the hot end of the device in such an application. The temperature of 400 K selected for second case study was selected (rather arbitrarily) with the aim of investigating how the different performance parameters vary with temperature. The parameters and values of the slow moving variables used for the case study are given in Table 1.

Fig. 6 shows the variation of the volume of material required per unit of exergy transfer with respect to D at different levels of exergy efficiency. Two important facts can be observed. The first is that more material is needed per kW of exergy transfer as D increases; thus the performance of the HX worsens. For $T_{avg} = 745K$, $D = 0.01m$ and $W = 0.99$ a volume of $17.16 \times 10^{-5}\,m^3$ per kW of exergy transfer is needed, while for a $D = 0.25m$ the volume needed at the same exergy efficiency increases to $70.41 \times 10^{-3}\,m^3$.

If the results presented in Fig. 6 are plotted in a log-log graph it is found that the curves have an average slope of 1.949, 1.922 and 1.869 for $W = 0.97$, 0.98 and 0.99 respectively, at a temperature of 745 K; while for a temperature of 400 K the slopes are 1.69, 1.769 and 1.811. The foregoing means that the volume per kW of exergy transfer nearly quadruples if the characteristic dimension D is doubled, which is a very important observation. This is in accordance with empirical conclusions from the HX industry which suggest that in general smaller dimensions yield a better performance.

The second important fact that can be observed in Fig. 6 is that more volume of material is required per kW of exergy transfer as

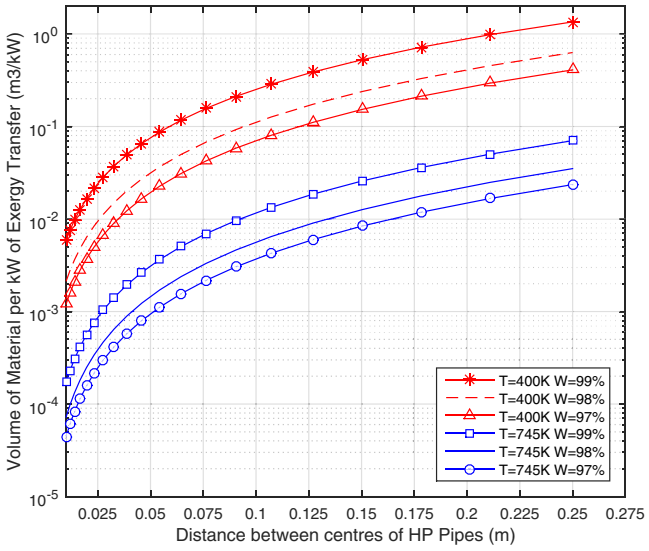

Fig. 6. Volume of material per kW of exergy transfer for different values of D.

the exergy efficiency level increases; i.e. a HX becomes (as expected) more expensive as it becomes more efficient. Additionally, it may be seen that the difference in volume from one value of W to another increases as W gets bigger; however, the increase is not as large as expected.

Fig. 7 shows the variation of the mass flow rates for different exergy efficiencies as the geometry is scaled up. Only $\dot{m}_{HP}$ values are shown as it has been established that $\dot{m}_{LP}$ is half as much, to have equivalent mass flow rates in both directions. The mass flow rates per pipe increase with D, as expected, because the geometry becomes bigger. For $T_{avg} = 745$ K, $D = 0.01m$ and $W = 0.99$ a $\dot{m}_{HP}$ of 24.26×10^{-5} kg/s is needed while for a $D = 0.25m$ and the same W the $\dot{m}_{HP}$ needed increases to 11.79×10^{-2} kg/s.

An interesting fact is that the mass flow rates increase as the exergy efficiency level (W) decreases. This occurs because as the geometry grows the ΔP in the pipes decrease; ΔP also decreases as W increases. The foregoing means that higher $\dot{m}$ are required to satisfy Eq. (5); in other words, the value of Z forces the system to increase $\dot{m}$ so that more exergy is lost due to pressure drops and the proportion established by Eq. (5) can be met.

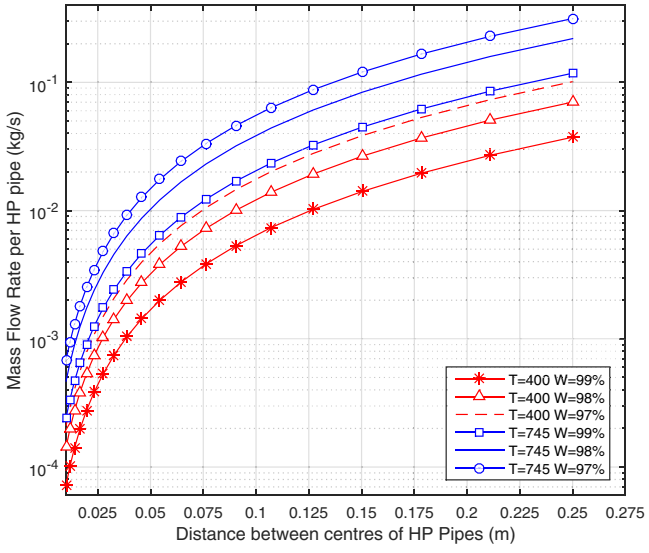

Fig. 7. Mass flow rate per HP pipe for different values of D.

Please cite this article in press as: B. Cárdenas, et al., Gas-to-gas heat exchanger design for high performance thermal energy storage, J. Energy Storage (2017), http://dx.doi.org/10.1016/j.est.2017.03.004

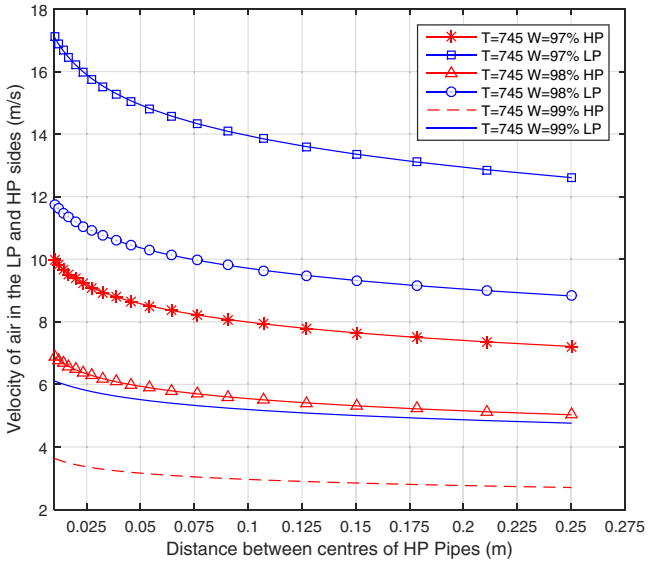

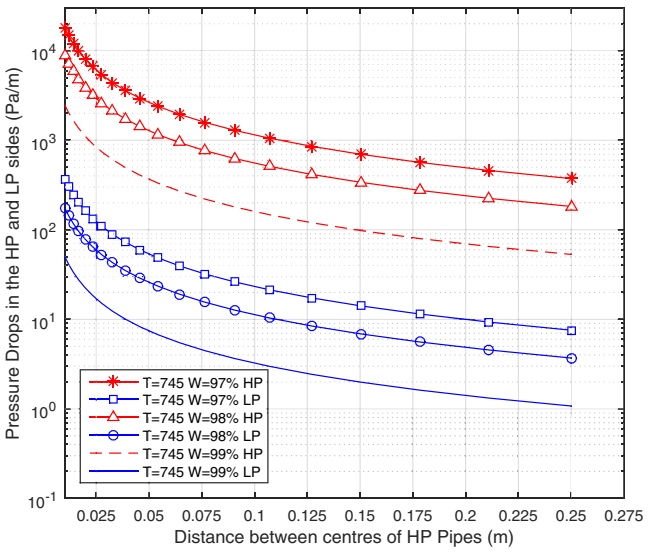

Fig. 10. Pressure drops in both streams (HP and LP) of the HX for different values of D, $T = 745$ K.

The behaviour of the velocities of both streams with respect to D for different levels of exergy efficiency at a T_{avg} of 745 and 400 K is shown in Figs. 8 and 9, respectively. Velocities decrease as the average temperature of the segment of HX decreases. In both cases, velocities decrease as D increases (despite increasing mass flow rates) due to bigger pipe diameters. The velocities of the streams decrease with increasing W because pressure drops (shown in Figs. 10 and 11) depend directly on them, so velocities have to be reduced in order to keep pressure-related exergy losses $\left(\dot{B}_{\Delta P}\right)$ to a minimum and achieve higher exergy efficiencies.

The variation of the temperature gradient (temperature change of the streams per unit length) of the segment of HX with respect to D at different levels of exergy efficiency is shown in Fig. 12. This parameter is of great importance as it provides information regarding the length of the HX. The temperature gradient decreases with increasing D because $\dot{m}$ increases. For $T_{avg} = 745$ K, $D = 0.25m$ and $W = 0.99$ a ∇T of 0.5354 K/m is observed while a considerably higher ∇T of 25.25 K/m is achieved for $D = 0.01m$ and $W = 0.99$.

Lower efficiencies exhibit a higher temperature gradient due to a larger heat transfer resultant from increased mass flow rates and heat transfer coefficients. This is in agreement with the results presented in Fig. 5, which states that more volume of material is required per kW of exergy transfer as the exergy efficiency increases.

The fraction of the outer perimeter of the HP pipes that is covered by flanges (λ) increases with D, which contributes to the larger volume per kW of exergy transfer observed for larger values of D. For a $T_{avg} = 745$ K, $D = 0.01m$ and $W = 0.99$ a λ of 0.027 is observed while λ increases to 0.285 for $D = 0.025m$ and $W = 0.99$. It should also be noted that for any given value of D, the HP pipes are less covered by flanges as the efficiency of the HX increases.

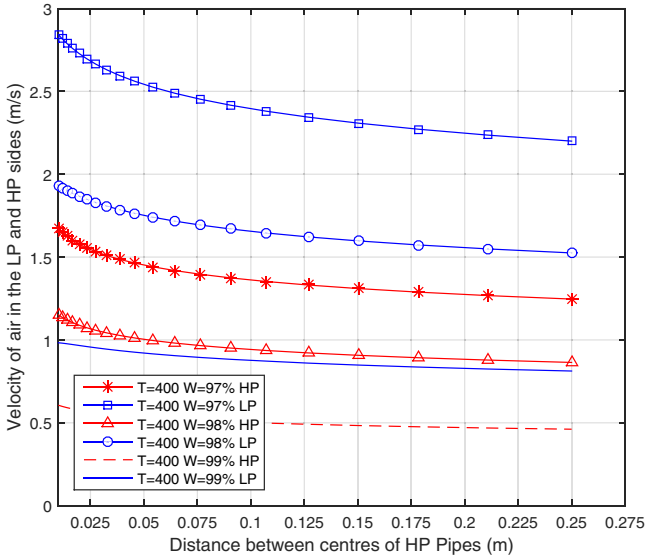

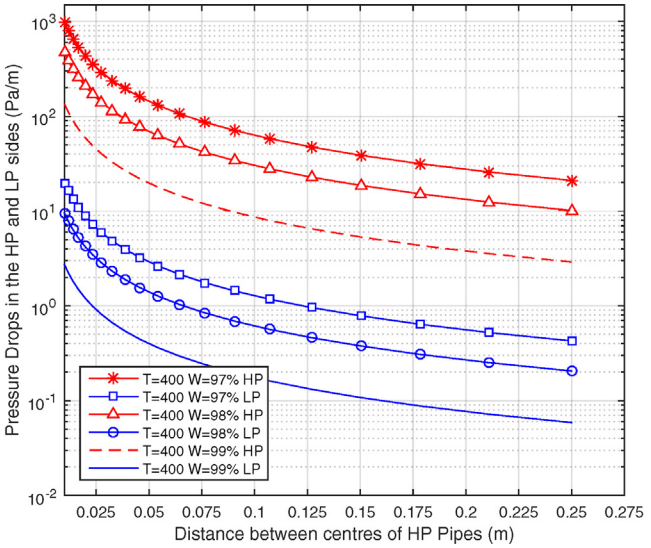

Fig. 11. Pressure drops in both streams (HP and LP) of the HX for different values of D, $T = 400$ K.

Please cite this article in press as: B. Cárdenas, et al., Gas-to-gas heat exchanger design for high performance thermal energy storage, J. Energy Storage (2017), http://dx.doi.org/10.1016/j.est.2017.03.004

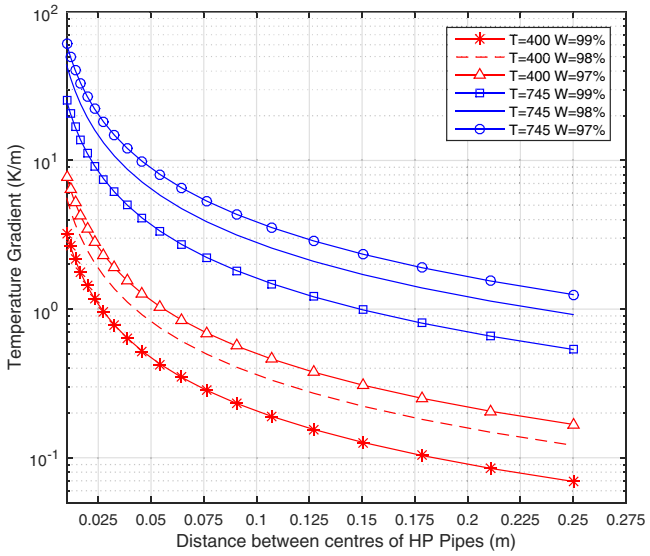

Fig. 12. Temperature gradient the streams for different values of *D*.

The aspect ratio (Area of HP pipe/Area of LP pipe) of the segment of HX increases with *D*, meaning that the HP pipes grow faster in comparison to LP pipes; however, the increase rate of this ratio decreases as *D* becomes larger. For a $T_{avg} = 745$ K, $D = 0.01m$ and $W = 0.99$ an aspect ratio of 0.0686 is observed while for a $D = 0.25m$ and $W = 0.99$ this value increases to 0.0719. For any given *D* this ratio is smaller for the higher efficiency designs because for achieving higher exergy efficiencies exergy losses due to pressure drops are minimized by reducing mass flow rates, which translates into smaller radii of the HP pipes and consequently a smaller aspect ratio.

One of the main benefits offered by the slow moving variables is the ability to carry out an optimization process through their fine tuning to improve the results obtained from the mathematical model. The optimization process employed, graphically shown by Fig. 13, is known as the one-factor-at-a-time method. It operates in the following way:

- The design for any *D* can be chosen as the initial point. A sweep through different values of *X* is done; maintaining *D* and the rest of the slow moving variables fixed to identify the value of *X* that yields the best performance.
- Thereafter, a sweep through different values of *Y* is done; maintaining fixed the *D*, *W*, *Z* and the newfound value of *X*, to identify the value of *Y* that yields the best performance.
- Subsequently, a sweep through different values of *Z* is done; maintaining fixed the *D*, *W* and the newfound values of *X* and *Y*, to identify the value of *Z* that yields the best performance.
- This completes the first iteration; the process is repeated until the values for *X*, *Y* and *Z* do not change.

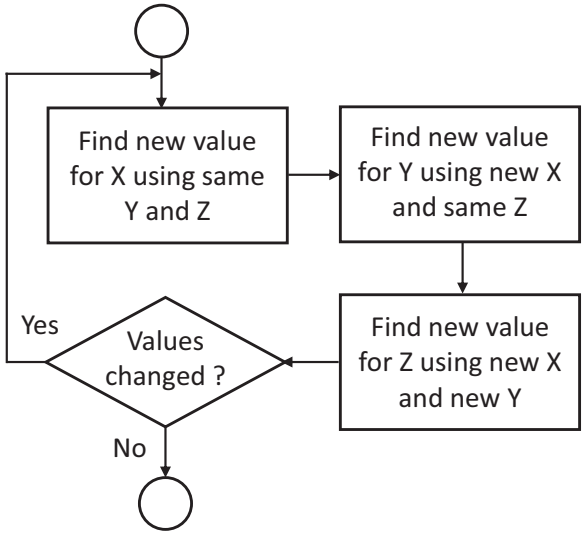

The design for $D = 0.01m$, $W = 0.99$ and $T_{avg} = 745$ K is used as the starting point for the one-factor-at-a-time optimization. A value 1.716×10^{-4} m^3/kW was obtained with the original values of the slow moving variables ($X = 1.0$, $Y = 0.5$, $Z = 0.5$) while with the revised values (after the first iteration) of $X = 4.25$, $Y = 0.2$ and $Z = 0.15$ a value of 8.795×10^{-5} m^3/kW has been achieved. Table 2 shows the improvement of the objective function $(V/\overline{B})$ after each step of the optimization as well as the combination of slow moving variables that yielded the best result.

The newfound values for the slow moving variables are used as starting point for a second iteration. Interestingly, the volume of material per unit of exergy transfer decreases continuously as *X* increases until reaching very small values. After $X = 11$ the LP stream presents a very small Reynolds number for being considered as a turbulent flow (<4000) [26] due to a considerable decrease in the velocity of the air. A turbulent flow is desired in order to maintain a healthy heat transfer in the pipes, therefore the sweep is stopped at $X = 11$. Subsequent sweeps were made for Y and Z and no change was found in their values, thus the optimization loop was concluded.

The final design for the cross-sectional area of the segment of the HX is obtained after the slow moving variables have been fine tuned. The geometric parameters and relevant performance metrics of the design generated for the case study are given in Table 3.

A volume of 8.485×10^{-5} m^3 of material per kW of exergy transfer with an exergy efficiency of 99% is achieved. For reference, a conventional shell-and-tube HX that operates between 820 and 350 K on the tube side with a pressure of 7 MPa requires of approximately 14.917×10^{3} m^3 per kW of exergy transfer with an efficiency of 95%. The volume obtained at the end of the one-factor-at-a-time optimization translates roughly into a cost of 53 €/kW (due to material only) considering an approximate cost of 80 €/kg for the steel powder for laser manufacturing [27]. Although the material used represents a large share of the total cost of a 3D printed part; additional fabrication costs such as labour (e.g. pre-processing of the job) and – specially – machine time are by no means negligible.

The current costing methods used for the fabrication of one-off and short run components are based on pre-established rates per unit volume that have already factored in the additional fabrication

Table 2
Reduction in volume per unit of exergy transfer after each step of the optimization.

Iteration	Slow moving variable changing	*X*	*Y*	*Z*	$V/\overline{B}$ (m^3/kW)
0	N/A	1	0.5	0.5	1.716×10^{-4}
1	*X*	4.25	0.5	0.5	1.669×10^{-4}
	Y	4.25	0.2	0.5	1.280×10^{-4}
	Z	4.25	0.2	0.15	8.795×10^{-5}
2	*X*	11	0.2	0.15	8.485×10^{-5}

Please cite this article in press as: B. Cárdenas, et al., Gas-to-gas heat exchanger design for high performance thermal energy storage, J. Energy Storage (2017), http://dx.doi.org/10.1016/j.est.2017.03.004

Table 3
Geometric parameters and performance metrics of the final design of the HX segment.

Operational parameters			Geometric parameters			Performance parameters		
X	11.0	–	D	0.01	m	W	0.99	–
Y	0.2	–	r_{HP}	5.701E^{-4}	m	ΔP_{HP}	2423.785	Pa/m
Z	0.15	–	t_{HP}	2.699 E^{-5}	m	ΔP_{LP}	4.4649	Pa/m
P_{HP}	5.0	MPa	t_{LP}	3.958E^{-6}	m	∇T	44.414	K/m
P_{LP}	101.325	kPa	L	4.403 E^{-3}	m	$V/\overline{B}$	8.485×10^{-5}	
T_{avg}	745	K	A_r	0.0239	–			
T_{HP}	749.967	K	λ	0.0063	–			
T_{LP}	740.032	K						
$\dot{m}_{HP}$	6.494×10^{-5}	kg/s						
$\dot{m}_{LP}$	3.247×10^{-5}	kg/s						
U_{HP}	2.739	m/s						
U_{LP}	1.593	m/s						

costs; so the intricacy of the design does not have a real impact on the end cost of the component. It is noteworthy that a further cost reduction can be achieved for hollow or perforated designs that allow different components to be built simultaneously within their cavities thus making a more efficient use of machine's running time. Both, material and indirect costs are expected to decrease as additive-manufacturing technologies mature. The standard additive manufacturing equipment commonly found nowadays can fabricate components with wall thicknesses down to one tenth of a millimetre, which renders most of the designs evaluated in the study as non-fabricable; however the capabilities of the machinery are rapidly improving and current state-of-the-art equipment is already capable of fabricating elaborate micro-scale structures [28].

It is important to emphasize that the design analyzed as a case study is just an example used to demonstrate the premise that it is possible to create designs for heat exchangers that are highly exergy-efficient and very cheap (due to the small volume of material required) if the constrains imposed by the limitations of traditional manufacturing methods are set aside.

5. Concluding remarks

Various new manufacturing techniques, such as additive manufacturing, have been developed in recent years; these methods allow the fabrication of intricate designs whose fabrication would not be possible or cost-effective through traditional methods.

A design for the cross-sectional area of a gas to gas heat exchanger based on an hexagonal mesh has been proposed with which a considerable volume (hence cost) reduction per unit of exergy transfer can be attained. This geometric configuration would be highly impractical to manufacture in a conventional way but could be easily built by means of modern techniques.

A segment of the heat exchanger that will work at an average temperature of 745 K was designed and optimized and a volume of steel as low as 84.846 cm^3 per kW of exergy transfer at a 99% exergy efficiency was obtained. Such geometry can be fabricated currently at competitive costs; and a further reduction in cost is expected as the new manufacturing methods mature.

The study has revealed a very important fact. The volume per kW of exergy transfer, which is one of the cost-driving factors, increases in nearly quadratic proportion with respect to the characteristic dimension (distance between centres of high pressure pipes) of the heat exchanger. This means that if the geometry is scaled up by doubling the distance between HP pipes, the volume of material per kW of exergy transfer will not be doubled – as intuition would suggest – but it will nearly quadruple.

The aforementioned observation may be true for other types of heat exchangers and with further analysis it could be regarded as a rule of thumb. It strongly suggests that the design of heat exchangers should aim towards such a small scale as possible for substantially increasing performance and reducing costs.

Acknowledgements

This work is an outcome of the UK-China NexGen-TEST collaborative research project; which has been funded by the UK Engineering and Physical Sciences Research Council (EPSRC) and the National Natural Science Foundation of China (NSFC). Special thanks to the organizing committee of the OSES 2016 Conference in Valletta, Malta in which this work was presented.

References

[1] K. Thulukkanam, Heat Exchanger Design Handbook, CRC Press, Florida, USA, 2013, pp. 1–15 J.
[2] A. Hadidi, A. Nazari, Design and economic optimization of shell-and-tube heat exchangers using biogeography-based (BBO) algorithm, Appl. Therm. Eng. 51 (2013) 1263–1272.
[3] S. Sanaye, H. Hajabdollahi, Multi-objective optimization of shell and tube heat exchangers, Appl. Therm. Eng. 30 (2010) 1937–1945.
[4] S. Sanaye, H. Hajabdollahi, Thermal-economic multi-objective optimization of plate fin heat exchanger using genetic algorithm, Appl. Energy 87 (2010) 1893–1902.
[5] H. Hajabdollahi, M. Tahani, M.H.S. Fard, CFD modeling and multi-objective optimization of compact heat exchanger using CAN method, Appl. Therm. Eng. 31 (2011) 2597–2604.
[6] H. Najafi, B. Najafi, P. Hoseinpoori, Energy and cost optimization of a plate and fin heat exchanger using genetic algorithm, Appl. Therm. Eng. 31 (2011) 1839–1847.
[7] V.K. Patel, R.V. Rao, Design optimization of shell-and-tube heat exchanger using particle swarm optimization technique, Appl. Therm. Eng. 30 (2010) 1417–1425.
[8] V.K. Patel, R.V. Rao, Thermodynamic optimization of cross flow plate-fin heat exchanger using a particle swarm optimization algorithm, Int. J. Therm. Sci. 49 (2010) 1712–1721.
[9] H. Sadeghzadeh, M.A. Ehyaei, M.A. Rosen, Techno-economic optimization of a shell and tube heat exchanger by genetic and particle swarm algorithms, Energy Convers. Manag. 93 (2015) 84–91.
[10] V.C. Mariani, A.R.K. Duck, F.A. Guerra, Coelho LdS, R.V. Rao, A chaotic quantum-behaved particle swarm approach applied to optimization of heat exchangers, Appl. Therm. Eng. 42 (2012) 119–128.
[11] O.E. Turgut, Hybrid chaotic quantum behaved particle swarm optimization algorithm for thermal design of plate fin heat exchangers, Appl. Math. Model. 40 (2015) 50–69.
[12] A. Hadidi, M. Hadidi, A. Nazari, A new design approach for shell-and-tube heat exchangers using imperialist competitive algorithm (ICA) from economic point of view, Energy Convers. Manage. 67 (2013) 66–74.
[13] M. Yousefi, R. Enayatifar, A.N. Darus, A.H. Abdullah, Optimization of plate-fin heat exchangers by an improved harmony search algorithm, Appl. Therm. Eng. 50 (2013) 877–885.
[14] Z. Wang, Y. Li, Irreversibility analysis for optimization design of plate fin heat exchangers using a multi-objective cuckoo search algorithm, Energ. Conv. Manage. 101 (2015) 126–135.
[15] M. Asadi, Y. Song, B. Sunden, G. Xie, Economic optimization design of shell and-tube heat exchangers by a cuckoo-search-algorithm, Appl. Therm. Eng. 73 (2014) 1032–1040.
[16] V. Patel, V. Savsani, Optimization of a plate-fin heat exchanger design through an improved multi-objective teaching-learning based optimization (MO-ITLBO) algorithm, Chem. Eng. Res. Des. 92 (2014) 2371–2382.
[17] R.V. Rao, V. Patel, Multi-objective optimization of heat exchangers using a modified teaching–learning-based optimization algorithm, Appl. Math. Model. 37 (2013) 1147–1162.
[18] D.K. Mohanty, Application of firefly algorithm for design optimization of a shell and tube heat exchanger from economic point of view, Int. J. Therm. Sci. 102 (2016) 228–238.
[19] M. Stewart, O.T. Lewis, Heat Exchanger Equipment Field Manual: Common Operating Problems and Practical Solutions, Gulf Professional Publishing, Oxford, UK, 2013, pp. 16–17.
[20] S. Haaland, Simple and explicit formulas for the friction factor in turbulent flow, J. Fluids Eng. 103 (1983) 89–90.
[21] W. Fox, P. Pritchard, A. McDonald, Introduction to Fluid Mechanics, John Wiley & Sons, New Jersey, USA, 2010, pp. 754.
[22] E.M. Shashi, Pipe strength and wall thickness, in: E. Shashi Menon (Ed.), Pipeline Planning and Construction Field Manual, Gulf Professional Publishing, Oxford, UK, 2011, pp. 105–121.
[23] W.S. Janna, Engineering Heat Transfer, CRC Press, Florida, USA, 2009, pp. 2–44.

Please cite this article in press as: B. Cárdenas, et al., Gas-to-gas heat exchanger design for high performance thermal energy storage, J. Energy Storage (2017), http://dx.doi.org/10.1016/j.est.2017.03.004

[24] E.W. Lemmon, R.T. Jabosen, S.G. Penoncello, D.G. Friend, Thermodynamic properties of air and mixtures of nitrogen, argon and oxygen from 60 to 2000 K at pressures to 2000 MPa, J. Phys. Chem. Ref. Data 29 (2000) 331–385.
[25] E.W. Lemmon, R.T. Jacobsen, Viscosity and thermal conductivity equations for nitrogen, oxygen, argon and air, Int. J. Thermophys. 25 (2004) 21–69.
[26] D. Bertsche, P. Knipper, T. Wetzel, Experimental investigation on heat transfer in laminar, transitional and turbulent circular pipe flow, Int. J. Heat Mass Tran. 95 (2016) 1008–1018.
[27] H. Piili, A. Happonen, T. Väistö, V. Venkataramanan, J. Partanen, A. Salminen, Cost estimation of laser additive manufacturing of stainless steel, Phys. Procedia 78 (2015) 388–396.
[28] Additive Manufacturing - Nanoscribe Gmbh". Nanoscribe.de, (2017) N.p., 2016. Web. 19 Jan..

Please cite this article in press as: B. Cárdenas, et al., Gas-to-gas heat exchanger design for high performance thermal energy storage, J. Energy Storage (2017), http://dx.doi.org/10.1016/j.est.2017.03.004